Bionic Optimization Design and Discrete Element Experimental Design of Carrot Combine Harvester Ripping Shovel

Wenqi Zhou [1], Xue Ni [1], Kai Song [1], Nuan Wen [1], Jinwu Wang [1,*], Qiang Fu [2], Mingjun Na [1], Han Tang [1] and Qi Wang [1]

1   College of Engineering, Northeast Agricultural University, Harbin 150030, China; zwq@neau.edu.cn (W.Z.); s211102049@neau.edu.cn (X.N.); s220701007@neau.edu.cn (K.S.); s200701701@neau.edu.cn (N.W.); nmj911@126.com (M.N.); tanghan@neau.edu.cn (H.T.);wangqi@neau.edu.cn (Q.W.)
2   School of Water Conservancy and Civil Engineering, Northeast Agricultural University, Harbin 150030, China; fuqiang0629@126.com
*   Correspondence: jinwuw@neau.edu.cn; Tel.: +86-0451-55191188

Abstract: Aiming at the common problems of the high working resistance, low soil disturbance, and high rates of missed extraction in the operation of carrot combine harvesters, a high-efficiency drag-reducing bionic soil-loosening shovel was designed in this study. The physical parameters of the soil and carrots were measured, and the bionic drag-reducing shovel was designed using the badger claw toe as a bionic prototype. The shovel wing structures were designed. Based on the EDEM discrete element simulation technology, a multi-element simulation model of the shovel–soil–carrot contact was established to determine the effects of the operating speed and sliding angle of the shovel handle on the resistance. The effects of the blade inclination angle and blade opening angle on the resistance, carrot extraction force, and soil disturbance rate were also studied. The results show that the resistance increases with an increase in operating speed. With a blade angle (α) and blade inclination angle (β) of 120.27° and 47.37°, respectively, the performance of the high-efficiency drag-reducing soil-loosening shovel is the best, with the resistance and carrot extraction force being 1908.76 N and 55.37 N, respectively. The virtual simulation experiment shows that this efficient drag-reducing shovel can effectively solve the problems of the low soil disturbance, high resistance, and high missing carrot rates of carrot combine harvester shovels, while also improving the harvesting quality and efficiency of carrot combine harvesters and meeting the agronomic requirements of carrot harvesting.

Keywords: carrot; soil-loosening shovel; bionic technology; discrete element method; efficient drag reduction

1. Introduction

The carrot is a delicious, crispy, and nutrient-rich vegetable. It can be eaten raw or cooked, as well as being juiced, salted, and dried or acting as fodder. Li Shizhen called it "the King of vegetable" [1]. The planting area and total production of carrots in China are the highest in the world [2], but most areas still use manual harvesting and semi-mechanized harvesting. Manual harvesting has the problems of a high labor intensity and low efficiency, while semi-mechanized harvesting has a high economic cost, which cannot meet the requirements of large-scale carrot harvesting.

Soil loosening is an important link of mechanized carrot harvesting, which directly affects the resistance and missing carrot rate [3]. Therefore, it is an effective way to promote mechanized carrot harvesting to improve the performance of carrot combine harvester shovels. Chong et al. [4] explored a wedge self-lubricating subsoiling shovel that was compared with a traditional subsoiling shovel under lubrication. The tillage resistance was reduced by 14.60~21.17%, and the average drag reduction rate was 18.28%, showing an obvious drag reduction effect. Askari et al. [5] developed a bending-wing subsoiling shovel

with bending angles of 10° and 20°. The test results showed that the soil disturbance and uplift area were increased by adding a wing to the subsoiling shovel handle, and the wing with a bending angle of 10° performed the best and, thus, can be used as an attachment for subsoiling shovels. Cheng et al. [6] analyzed the effects of a chisel shovel, arrow shovel, and wing shovel on the soil breakage rate and soil disturbance. The results revealed that the shape of the bionic soil shovel had an important impact on the soil disturbance process, and the wing subsoiling shovel presented the highest soil disturbance and highest resistance. Aday et al. [7] investigated the influence of different blade angles on the resistance of a subsoiling shovel. When the blade angle was 25°, the resistance, disturbance area, and energy utilization efficiency were superior to those obtained with other angles. However, there are differences in the soil quality of different carrot-planting regions, as well as in the structure and material of soil-loosening shovels. The above studies did not conduct corresponding experimental studies on the soil of carrot-planting areas in the northeast black land, so the corresponding subsoiling shovels cannot be applied to carrot harvesting in the northeast black land.

Bionic design can effectively improve the performance of soil-loosening components. Wei et al. [8] took bamboo rats and antlion larvae, which are good at digging, as the bionic objects to build 3D surfaces of the bamboo rat paw and antlion larva back through reverse engineering and designed a slant column subsoiling shovel, which effectively reduced the subsoiling resistance, with a maximum reduction of 12.92%. Qiu et al. [9] designed a corrugated bionic subsoiling shovel by using the resistance reduction mechanism of the corrugated surface of earthworms. Through the simulation analysis of ANSYS/LS-DYNA software, they found that the tillage resistance of the corrugated bionic subsoiling shovel was significantly lower than that of the original subsoiling shovel, the theoretical service life was longer than that of the original subsoiling shovel, and the working performance was more reliable than that of the original subsoiling shovel. Gowripathi et al. [10] selected the crank–rocker mechanism for vibrating subtillage in banana planting. The trajectory required by the crank–rocker mechanism of the bionic vibrating subsoiling shovel machine was examined via kinematic analysis. The speed and acceleration required for operating the tillage tool were determined. The experiment indicated that the working efficiency of the bionic vibrating subsoiling shovel was improved by about 30% compared to that of the traditional subsoiling shovel, which greatly improved the planting rate of bananas. Li et al. [11] developed a bionic subsoiling component based on the brown bear paw and studied the effects of factors such as the bionic subsoiling angle and tillage depth on the tillage resistance and soil disturbance. Zhang et al. [12] explored a bionic subsoiling shovel with the head of the sandfish lizard as the bionic prototype by using reverse engineering technology. The discrete element method was applied for analysis, finding that the bionic soil-loosening shovel required a low traction force, and its drag reduction rate was 8.34~19.31%. Q et al. [13] designed a bionic subsoiling shovel based on the shape of the armadillo claw, aiming to effectively break the soil by reducing its friction and adhesion to cutting tools. The claw toe contour was obtained by using CAD technology. The effectiveness of the bionic design was verified by comparing its results with the results obtained from a traditional subsoiling shovel. The bionic design reduced the horizontal and vertical drag by 36.6% and 58%, respectively. Zhang et al. [14] researched a drag-reducing subsoiling shovel with an exponential function curve-type blade by fitting the paw curve of a mouse. The test results showed that the bionic design significantly reduced the tillage resistance of the subsoiling shovel. S et al. [15] evaluated the sustainable subsoiling performance of a bionic integral subsoiling shovel (SIB), multiple plows (M), a subsoiling shovel (S), a disc plow (AD), and a disc harrow (Ra). It was found that the SIB and M had a greater working width and required a greater pulling force and less fuel consumption per hectare. The operating speed of the SIB had a direct impact on its operating performance, and the performance was 33.8% better than that of a traditional subsoiling shovel. The SIB represents a sustainable option for the primary tillage of soil, which can be an alternative to traditional tillage. Zhang et al. [16] designed and produced the variable curvature

drag-reducing structure of a subsoiling shovel by using the contours of the vole paw toe as a bionic prototype curve, which can allow the machine to have a low working resistance within a wide range of working speeds and achieve the goal of subsoiling drag reduction under high-speed operation.

The position of the bionic soil shovel installation in carrot combine harvesters is located under the pulley, the shovel handle is located under the machine and the frame hinges, and the shovel wing and bionic shovel are located under the pulley and the shovel handle solid connection. The whole machine works under the traction of the tractor's forward movement, with the shovel tip penetrating the soil and dragging the soil particles along the inside of the bionic shovel tip. The soil between the carrot rows is disturbed by the spatula wing to reduce the adhesion between the carrots and the soil. The spatula handle breaks the surface soil, and the soil particles slide backward along the surface of the spatula. When the spatula tip moves to the center of the carrot, the carrot tassel is in an upright state through the rotation of the harvester, and under the action of the conveyor belt, the carrot tassel is clipped to the rear. As a result, the carrot-loosening, digging, and conveying operations are completed. However, due to the poor soil disturbance performance of carrot combine harvesters, their resistance is high, the carrot leakage rate is high, and the working efficiency is low. Moreover, a special soil shovel has not been developed in combination with the carrot production mode and the requirements of harvesting agriculture, and this affects the working quality and power consumption of the machine.

The performance of the soil-loosening shovel directly affects the quality of carrot harvesting. The high resistance leads to an increase in power consumption, and the poor disturbance of the soil-loosening shovel increases the missing carrot rate. In order to effectively improve the soil disturbance, the structure of the soil-loosening shovel wing is typically increased, but this also significantly increases its resistance [17–19]. Therefore, the structural size of the soil-loosening shovel wing is optimized to effectively reduce the resistance under the premise of increasing soil disturbance. In this study, the physical parameters of the soil and carrots were measured in Qingfeng Village, Harbin City, Heilongjiang Province, China, including the soil water content, soil bulk density, soil firmness, carrot geometric parameters, root tensile strength, and pulling force. Taking the badger claw structure as a bionic prototype, the external outline of the badger claw was extracted using a 3D contact-free reverse scanner, and a 3D digital design was carried out. The surface structure of the creature and its low-resistance and low-disturbance characteristics were completely extracted and optimized, and then manufacturing and production were complemented by metal 3D printing technology, so as to design a bionic drag-reducing subsoiling shovel with a badger claw structure for carrot harvesting. A discrete element model of the soil, carrots, and soil particles was constructed, and a virtual simulation test was carried out to explore the interaction between the bionic drag-reducing subsoiling shovel, soil, and carrots. A single-factor test was performed with the operating speed, sliding angle of the shovel handle, opening angle of the blade, and inclination angle of the blade as the test factors; and the resistance, carrot-pulling force, and soil disturbance were the test indexes. This study aimed to explore the effect of the structural parameters of a highly efficient drag-reducing bionic soil-loosening shovel on its operation quality when used on a carrot combine harvester, so as to solve the problems of the low soil disturbance, high resistance, and high missing carrot rate of soil-loosening shovels and improve the harvest quality and efficiency of carrot combine harvesters.

2. Materials and Methods

The physical parameter measurement of the soil and carrots is an important means to improve the adaptability and performance of carrot combine harvesters. In this section, the black soil of Qingfeng Village (46°42′38.7″ N, 129°58′31.1″ E), Harbin City, Heilongjiang Province, and the carrot "Hongsheng Qicun" planted in this area were selected as the research objects to determine the physical parameters, such as the soil solidity, water content, bulk density, and carrot geometric and mechanical parameters. This can provide a

theoretical foundation for the structural design of a high-efficiency drag-reducing bionic soil-loosening shovel, as well as providing the theoretical basis and boundary conditions for simulation analysis.

2.1. Measurement of Soil Physical Parameters

2.1.1. Measurement of Soil Water Content

The soil water content is an important physical parameter of soil, reflecting the ratio of soil to water. Changes in the soil water content will cause changes in the soil mechanical properties, such as cohesion and plasticity [20]. In the process of mechanized carrot harvesting, the soil water content has an important effect on the carrot-pulling force and directly affects the carrot harvesting quality. Due to its easy operation and high precision, this study adopted the drying method to measure the water content of the soil in the experimental field [21]. In the experimental field, the tillage layer (0~100 mm), plow layer (100~200 mm), and subsoil layer (200~300 mm) of 5 sites were randomly selected for soil sampling [22], labeling the soil sampling box and calculating the soil water content according to Equation (1):

$$S_m = \frac{m_1 - m_2}{m_2 - m_0}$$

(1)

where S_m is the soil water content, %; m_0 is the mass of the empty soil box, g; m_1 is the total mass of the soil and box before drying, g; m_2 is the total mass of the soil and box after drying, g.

According to the measured data and Equation (1), the average soil moisture content of the plow layer in the test field was 11.63%, the average soil moisture content of the plow bottom layer was 14.41%, and the average soil moisture content of the core soil layer was 18.21%. The soil water content and soil viscosity at the test site were high. Under these conditions, the soil is in close contact with the carrot roots, and this is not conducive to carrot harvesting.

2.1.2. Measurement of Soil Bulk Density

The mass or weight of soil per unit volume under the natural state is called the soil bulk density [23]. The soil bulk density reflects the bulkiness and plasticity of soil, as well as the contact state between the soil and carrots. The higher the soil bulkiness, the easier it is for carrots to be harvested; otherwise, carrots are hard to harvest. In order to construct the theoretical parameter model of the soil–crop accurately, the soil bulk density of each tillage layer was measured. As the soil of the test field was medium clay, which is soft and can easily clump, the cutting ring method was used in this paper to measure the soil bulk density of the test site [24]. According to Equation (2), the soil bulk density of different plow layers was calculated:

$$d_{vi} = \frac{M_i \times 100}{V(100 + W_i)}$$

(2)

where d_{vi} is the soil bulk density of the ith soil sample, g·cm^{-3}; V is the cutting ring volume, cm^3; M_i is the mass of the ith soil sample, g; and W_i is the soil water content, %.

The average soil bulk density of the cultivated layer in the test field was 1.236 g/cm^3, the soil bulk density of the plow bottom layer was 1.433 g/cm^3, and the soil bulk density of the core soil layer was 1.508 g/cm^3.

2.1.3. Measurement of Soil Firmness

Soil firmness is the compactness of the soil particle arrangement, also known as soil hardness [25]. In clay soil, carrots are in close contact with the soil particles, resulting in an increased pulling force being required for carrot harvesting and an increased missing carrot rate. Soil firmness also has a significant influence on the resistance of soil-loosening shovels. The average firmness of the cultivated layer in the test field was 786 kPa, that of the plow bottom layer was 1536 kPa, and that of the core soil layer was 2632 kPa.

2.2. Measurement of Carrot Physical Parameters

2.2.1. Measurement of Carrot Geometric Parameters

The geometric parameters of carrots are a significant basis for designing soil-loosening shovels of carrot combine harvesters [26,27]. The key geometric parameters of carrots were measured, including the length of the carrot stem and leaf, root length, maximum root diameter, minimum root diameter, diameter of the tassel junction, and diameter of the stem and leaf. The main distribution interval of the carrot stem and leaf length was (350, 600) mm; the main distribution interval of the root length was (125, 225) mm; the main distribution interval of the maximum root diameter was (27, 51) mm; the main distribution interval of the minimum root diameter was (2, 8) mm; the main distribution interval of the diameter of the tassel junction was (9, 15) mm; and the main distribution interval of the stem and leaf diameter was (6, 22) mm.

2.2.2. Measurement of Carrot Root Tensile Properties

In order to solve the common problem whereby the carrot tassels break during carrot combine harvesting, leading to high missing carrot rates, the tensile characteristics of the carrot roots were measured [28,29]. A metal probe was vertically inserted into the soil surface for measurement using an SL-TYA firmness tester. The indicator number of the tester was read after it became stable. The tensile strength of the carrot stem and leaf, the maximum breaking force of the tassel junction, and the breaking position were selected as measuring indexes. The breaking condition of the carrots was determined by adjusting the loading speed and the carrot-clamping position of the universal testing machine. According to Equation (3), the tensile strength of carrot roots under different loading speeds was calculated:

$$\sigma_i = \frac{4F_i}{\pi D_i^2} \tag{3}$$

where σ_i is the tensile strength of the ith carrot root, Pa; F_i is the peak pulling force of the ith carrot tassel junction fracture, N; and D_i is the diameter of the ith carrot tassel junction fracture, mm.

The test results of carrot tensile strength are shown in Table 1. The maximum breaking force of the carrot stem and leaf decreases along the direction of cellulose and decreases with the decrease in the diameter of the carrot stem and leaf. The tensile strength of the carrot stem and leaf increases with the increase in loading speed and decreases with the increase in clamping height.

Table 1. Test results of carrot tensile strength.

Loading Speed \ Clamping Height	Statistical Indicators	0–50	50–100	100–150	150–200
2 mm/s	Breaking force (N)	260.76	245.31	215.65	176.33
	Tensile strength (10^5 Pa)	8.17	7.66	6.21	5.34
	Diameter of breaking part (mm)	16.14	13.25	12.76	10.93
3 mm/s	Breaking force (N)	276.53	263.71	259.49	246.86
	Tensile strength (10^5 Pa)	9.15	8.77	8.13	7.69
	Diameter of breaking part (mm)	17.92	16.35	13.68	11.49
4 mm/s	Breaking force (N)	289.66	276.38	269.57	254.36
	Tensile strength (10^5 Pa)	10.54	9.81	8.76	7.33
	Diameter of breaking part (mm)	19.16	18.65	17.95	16.32

2.2.3. Measurement of Carrot-Pulling Force

The carrot-pulling force is an important evaluation index to measure the performance of soil-loosening shovels during carrot mechanized harvesting [30]. The research on the cohesion between carrots and soil and the carrot breaking conditions provides a theoretical basis for the subsequent structural design and virtual simulation test of soil-loosening shovels.

Carrots of similar size were selected to measure the pulling force. A transparent adhesive strip was fixed on the upper part of the carrot stem and leaf, and the pull meter was pulled to make the carrot move slowly along the pulling direction. The peak pulling force of the carrot was obtained by observing the indicator of the pull meter.

It can be seen in Tables 2 and 3 that when the extraction angle exceeds 35°, the carrot extraction force increases significantly; when the soil-loosening depth exceeds 200 mm, the carrot extraction force tends to be stable; and when the soil-loosening depth exceeds 250 mm, the carrot extraction force reaches its minimum value.

Table 2. Results of carrot extraction force test at different angles.

Extraction Angle (°)	Extraction Force Max (N)	Extraction Force Min (N)	Extraction Force Average (N)
5°	276.85	197.63	215.37
15°	254.21	201.58	230.69
25°	266.39	187.37	231.78
35°	295.47	207.85	235.68
45°	284.36	212.68	255.17

Table 3. Test results of carrot extraction force with different soil depths.

Loose Soil Depth (°)	Extraction Force Max (N)	Extraction Force Min (N)	Extraction Force Average (N)
0	298.62	186.36	226.69
50	134.58	87.26	96.88
100	98.61	58.35	73.21
150	84.29	46.38	65.44
200	76.28	41.96	58.31
250	75.77	39.48	56.69

The results indicate that the effect of carrot pulling is closely related to the pulling angle and the soil-loosening depth. The carrot-pulling force increases with the increase in the carrot-pulling angle. The soil-loosening depth greatly impacts the carrot-pulling force; that is, the carrot-pulling force decreases with the increase in soil-loosening depth.

2.3. Structure Design of Bionic Soil-Loosening Shovel Based on the Geometric Structure of the Badger Claw Toe

The badger, which has curved, conical, hard, and powerful claw toes, has a strong ability to plow. Its front claw toe presents excellent drag-reducing ability [31,32]. In this study, the special curve structure of the inner side of the badger claw toe was combined with its complex surface microstructure through the bionics principle, which was applied to the structural design of the soil-loosening shovel of a carrot combine harvester, so as to achieve the purpose of drag reduction. This study also selected the stronger middle finger of the five claw toes of a naturally dead badger as the bionic object for the design of the soil-loosening shovel, as shown in Figure 1.

Figure 1. Photo of badger sampling.

The badger claw toe has a complex microscopic curve structure. The 3D data of the claw toe were obtained using a non-contact method. The non-contact 3D scanner EinScan Pro 2x produced by the SHINING 3D Company was used to scan the claw toe. Point cloud smoothing and clutter elimination optimization were performed on the obtained claw toe point cloud data, so as to obtain smooth and accurate point cloud data. Then, the optimized point cloud model was wrapped and filled using Geomagic Design X software to obtain the 3D model of the badger claw toe [33–35], as shown in Figure 2.
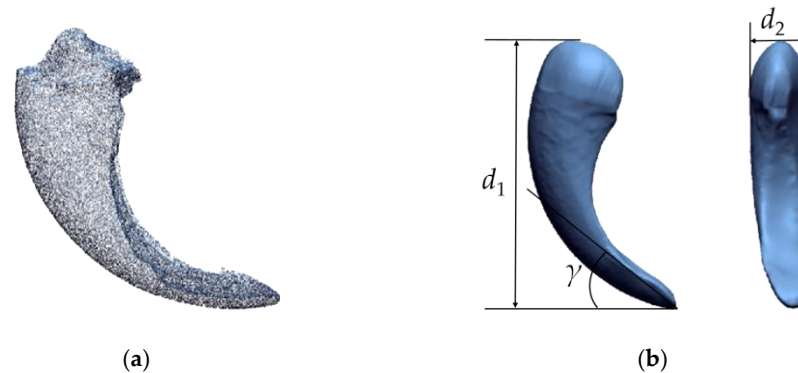

(**a**)   (**b**)

Figure 2. Point cloud and 3D model of the badger claw: (**a**) point cloud map and (**b**) 3D model diagram.

In order to explore the drag reduction mechanism of the inner structure of the badger claw toe, the curve equation of the inner side of the badger claw toe was fitted and analyzed [36]. The obtained 3D model of the badger claw toe was imported into Solidworks software. Then, we took sampling points in sequence and recorded the data. The sampling data were imported into the function plotting software Origin for curve fitting, so as to obtain the curve fitting equation of the inner side of the claw toe:

$$y = 110.28e^{(-x/37.45)} + 184853.84e^{(-x/2.11)} + 10.44 \qquad (4)$$

The correlation coefficient of the fitting curve was $R^2 = 0.95815$. The 3D model of the badger claw toe was imported into Solidworks software for proportional amplification. In order to ensure the adaptability of the model, 10-times magnification was selected, and the soiling angle of the soil-loosening shovel was $\gamma = 25°$ according to the planting mode and growing characteristics of carrots and the existing structural parameters of the soil-loosening shovel and the soiling angle [37]. At this point, the soiling depth was $d_1 = 97.8$ mm, and the soiling width was $d_2 = 68$ mm.

The bionic soil-loosening shovel is made of steel, with a density of 7.85 g/cm^3, a volume of 30.87 cm^3, and a mass of 242.3 g. Due to the small volume and relatively small mass of bionic shovels, the soil disturbance is low.

Therefore, the structural size of the soil-loosening shovel wing was optimized to effectively reduce the resistance under the premise of increasing soil disturbance. In addition, a mechanical model was established to analyze the factors affecting the resistance, providing a theoretical basis for the subsequent discrete element simulation tests. The structure of the bionic soil-loosening shovel is shown in Figure 3.
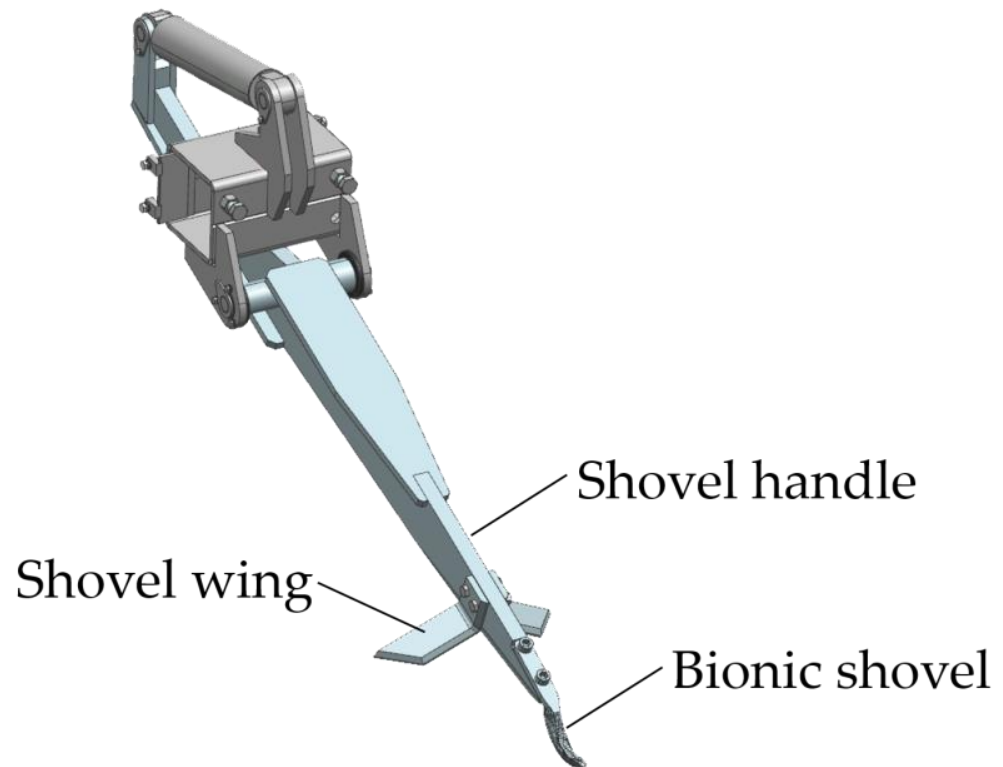

Figure 3. Structure of the bionic soil-loosening shovel.

2.4. Establishment of Discrete Element Model of the Soil-Loosening Shovel, Carrots, and Soil Particles

In this study, a multi-element coupling model was constructed by taking the 3D model of the soil-loosening shovel, the test field, and a carrot as carriers to analyze the performance rule of the soil-loosening shovel. In order to obtain the optimal structural parameters of the soil-loosening shovel wing, a virtual simulation test was carried out based on discrete element software with the opening angle (α, the angle between the left and right wings of a loose shovel) and inclination angle (β, the angle between the wings of a loose shovel and the horizontal plane) of the soil-loosening shovel wing as the test factors; and the resistance, carrot-pulling force, and soil particle disturbance served as the test indexes. Solidworks was used to carry out solid proportional modeling of the soil-loosening shovel, and the model was imported into EDEM software. According to the operation requirements, the material of the soil-loosening shovel is 65 Mn steel. Its Poisson ratio and shear modulus were set in EDEM software. The carrot 3D model was imported into the DEM-simulated soil trough through Geometries. The virtual simulation model of the soil-loosening shovel is shown in Figure 4, and the carrot is shown in Figure 5.
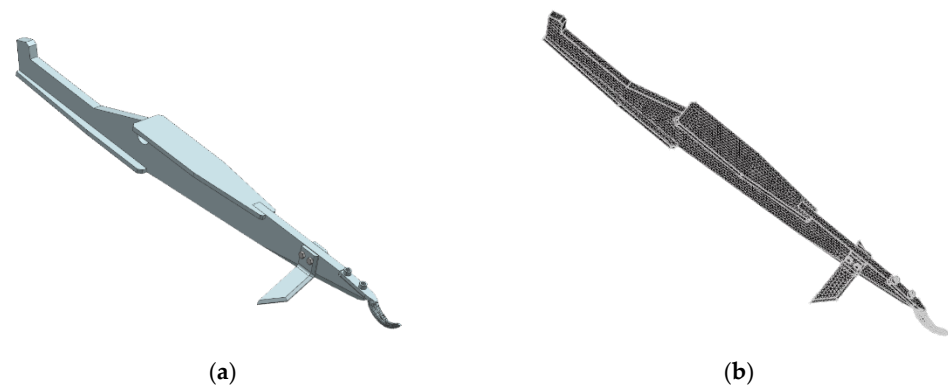
Figure 4. Model of the soil-loosening shovel virtual simulation: (**a**) filled format and (**b**) mesh format.
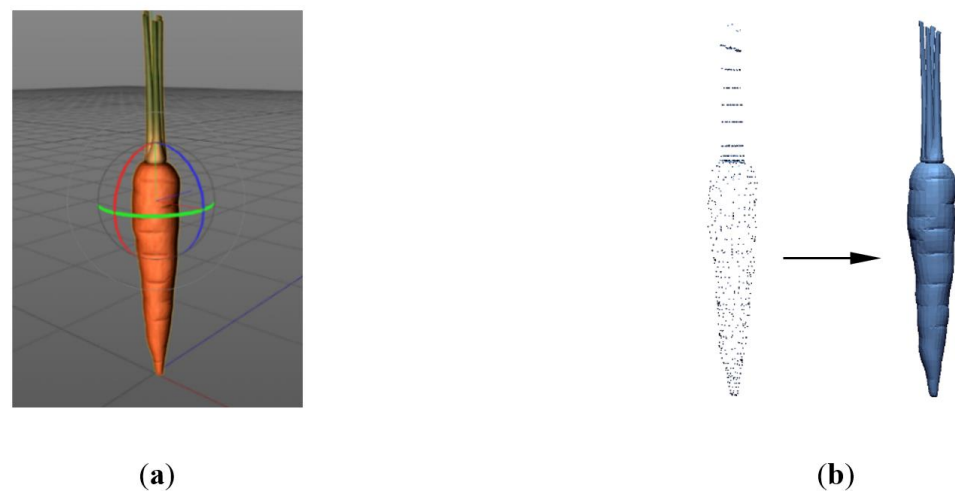

(**a**) (**b**)

Figure 5. Model of the carrot point cloud: (**a**) point cloud map and (**b**) 3D model.

In order to accurately simulate the contact between the carrot and soil and extract an accurate carrot model, the EinScan Pro 2x non-contact 3D scanner was used to scan the carrot, establish 3D carrot models, and import them into the EDEM simulated soil trench. The basic size of the soil trench (length × width × height) was set to 400 mm × 400 mm × 500 mm in the model. According to the early measurement of the tillage layer, the virtual soil trench was stratified, namely the tillage layer, plow bottom layer, and subsoil layer. The simulation model is shown in Figure 6.
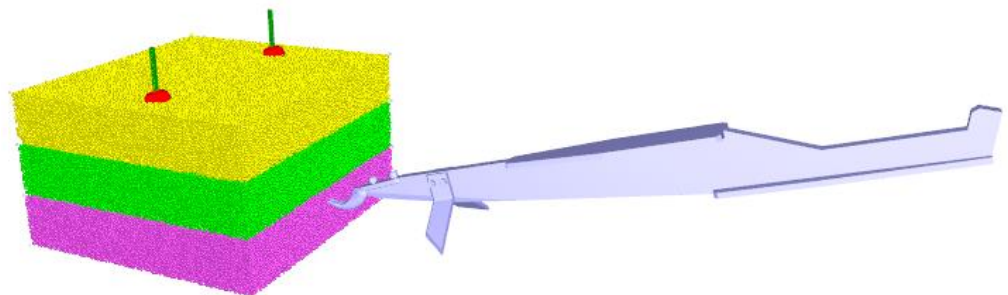

Figure 6. Virtual soil trench modeling.

In order to accurately simulate the contact state of the soil-loosening shovel–soil–carrot, the bonding force of the soil particles is mainly set according to their internal cohesion characteristics. The complex bond and fracture relationships among the soil particles were simplified into the contact model between soil and soil as Hertz–Mindlin JKR, the contact model between soil and carrot as Hertz–Mindlin JKR, and the contact model between

soil and bionic shovel as Hertz–Mindlin no slip. A virtual soil trench was established using EDEM software. The soil particle model was generated in a virtual particle factory according to the probability distribution percentage of the soil properties in each layer. A virtual plane with the same size as the upper surface of the virtual soil trench was established to make it move from top to bottom. The virtual plane dropped 1 mm at a rate of 20 mm/min to compact the soil [38]. During the movement, the plane contacted the soil particles and compacted the virtual soil trench, so as to keep the simulation environment consistent with the actual soil.

2.5. Simulation Parameter Setting

The established 3D model of the soil-loosening shovel and carrot was imported into EDEM software, placing the 3D model in the specified position, using moving and rotating commands. The root was used to construct the soil-loosening shovel–soil–carrot coupling contact model through the EDEM preprocessing module. The specific parameters are shown in Table 4 [39,40].

Table 4. Basic parameters of the discrete element model.

Parameter	Value
Soil–soil recovery coefficient, e_1	0.2
Soil–soil kinetic friction coefficient, e_2	0.4
Soil–soil static friction coefficient, e_3	0.3
Soil–65Mn recovery coefficient, f_1	0.3
Soil–65Mn kinetic friction coefficient, f_2	0.5
Soil–soil static friction coefficient, f_3	0.05
Soil–carrot recovery coefficient, b_1	0.5
Soil–carrot kinetic friction coefficient, b_2	0.43
Soil–carrot static friction coefficient, b_3	0.2

2.6. Evaluation Index of Virtual Simulation

Through the virtual simulation experiment, the combination of the optimal operating parameters and optimal structural parameters of the soil-loosening shovel wing was explored, providing the theoretical basis for the structural design of the soil-loosening shovel for a carrot combine harvester. In order to quantify the missing carrot rate and forward power consumption of the machine, the missing carrot rate was converted into a carrot-pulling force in the virtual simulation, and the forward power consumption was converted into resistance and output in real time through the EDEM postprocessing command.

(1)   Resistance of the soil-loosening shovel

In this study, a DS2 digital force gauge (Dongguan Zhiqu Precision Instrument Co., LTD., Dongguan City, Guangdong Province, China) was used to measure the resistance of the bionic soil-loosening shovel at different speeds. At the same time, EDEM software was selected to determine the resistance of the bionic soil-loosening shovel at different times [41]. The data were output through postprocessing, and the figure of the resistance variation in each stage was generated using Excel software.

(2)   Carrot-pulling force

When pulling carrots, the bond between the carrots and soil is relatively strong, resulting in the fracture of the carrot tassels, leading to an increase in the missing carrot rate [42]. Therefore, the carrot-pulling force is an important index to test the performance of soil-loosening shovels. When the shovel moves below the carrot, the soil bulkiness reaches its peak, corresponding to the minimum carrot-pulling force. At this time, the carrot begins to move upward. During the movement, soil particles adhere to the carrot surface due to the large bonding force between the carrot and soil.

(3) Soil particle disturbance coefficient

The soil disturbance coefficient is commonly used as the index to evaluate the soil particle disturbance effect [43]. The accumulation contour of soil on the surface after soil loosening to the bottom of the trench after the actual deep loosening is taken as the ratio of the cross-sectional area of the soil-disturbed ridge and the cross-sectional area from the surface before soil loosening to the theoretical bottom of the trench, which is the soil disturbance coefficient, and its equation is as follows [44,45]:

$$y = \frac{A_s}{A_q} \times 100\% \tag{5}$$

where y is the soil disturbance coefficient, %; A_s is the cross-sectional area from the ground surface to the real bottom of the trench after subsoiling, mm^2; and A_q is the cross-sectional area from the ground surface to the theoretical bottom of the trench before subsoiling, mm^2.

The larger the soil disturbance coefficient, the better the subsoiling effect, the greater the benefit to the pulling and harvesting of carrots, and the higher the quality of the harvested carrots.

3. Results and Discussion

3.1. Effects of Operating Speed (v) on Resistance

Referring to the common operating requirements of carrot harvesters and the research of relevant scholars [46–48], the operating speed range was selected as (2.16 km/h, 2.52 km/h, 2.88 km/h, 3.24 km/h, and 3.60 m/h). The resistance of the bionic subsoiling shovel at different speeds was measured using a DS2 digital force gauge, as shown in Figure 7.
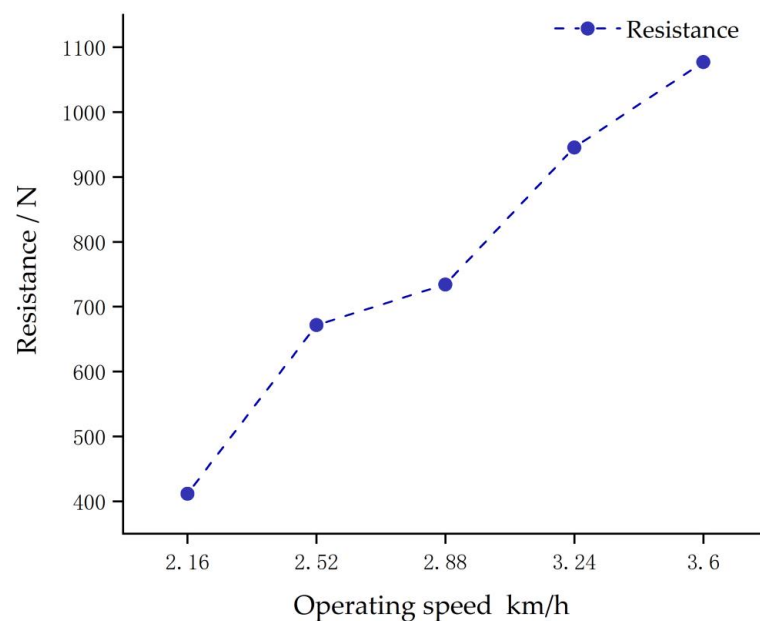

Figure 7. Resistance analysis of the soil-loosening shovel.

In Figure 8,when soil particles contact the surface of the bionic soil-loosening shovel, there is a relative velocity (v), which can be decomposed into the tangential velocity (v_1) and normal velocity (v_2). The normal velocity (v_2) is converted into resistance (F_1), which hinders the forward movement of the bionic soil-loosening shovel. The resistance (F_1) can be decomposed into the horizontal resistance (F_{d1}) in the horizontal direction and vertical resistance (F_{v1}) in the vertical direction. The vertical resistance (F_{v1}) produces positive pressure on the bionic soil-loosening shovel, which is also represented by the friction force exerted on the bionic soil-loosening shovel. The resistance (F_{j1}) is composed

of the horizontal resistance (F_{d1}) and the horizontal component (F_{j1}) of the friction force acting on the bionic soil-loosening shovel.

$$v_2 = v \cos \delta \tag{6}$$

$$F_{d1} = F_1 \cos \delta = m \frac{v_2 - v_0}{t} \cos \delta = m \frac{v}{t} (\cos \delta)^2 \tag{7}$$

$$F_{f1} = \mu_1 F_{v1} (\sin \delta)^2 = \mu_1 F_1 (\sin \delta)^3 \tag{8}$$

$$F_{j1} = F_{d1} + F_{f1} = \frac{mv \cos \delta}{t} \cdot \left(\mu_1 \sin^3 \delta + \cos \delta \right) \tag{9}$$

where m is the particle mass, kg; v is the initial operating speed, m/s; v_0 is the final forward velocity, m/s; t is the action time, s; a is the acceleration, m/s^2; and μ_1 is the friction coefficient between the bionic soil-loosening shovel and soil.

v—operating speed
v_1— tangential velocity
v_2—normal velocity
F_1—resistance
F_{d1}—horizontal resistance
F_{v1}—vertical resistance
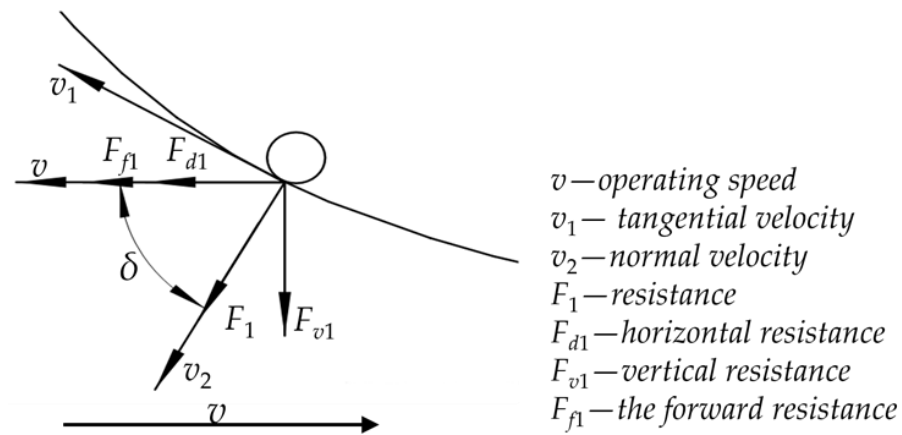F_{f1}—the forward resistance

Figure 8. Comparative analysis of mechanics between soil particles and the tip of the soil-loosening shovel.

According to Equation (9), $\mu_1 \sin^3 \delta$ is much smaller than $\cos \delta$, meaning that Equation (9) can be simplified as follows:

$$F_{j1} = m \frac{v}{t} \cos^2 \delta \tag{10}$$

As can be seen in Equation (10), the resistance (F_{j1}) increases with the increase in operating speed. As shown in Figure 9, in the initial stage of interaction between the soil particles and soil-loosening shovel moving at the same speed, the resistance increases rapidly with the increase in time. The soil particles move with variable acceleration along the curve of the inner side of the bionic soil-loosening shovel and fly out from the top of the bionic soil-loosening shovel, significantly decreasing its resistance. When the simulation operation reaches between 0.5 and 0.8 s, the resistance increases rapidly, mainly because the soil-loosening shovel gradually enters the virtual soil trench and squeezes the internal soil, which destroys the soil bonds and consumes a lot of energy, resulting in a steady increase in resistance. When the simulation operation comes to 1.1~1.2 s, the resistance increases sharply to its peak value, mainly because the soil-loosening shovel wing penetrates the soil particles, and the soil disturbance is enhanced, resulting in a large number of soil particle bond fractures. When the simulation runs to 1.3 s, the soil-loosening shovel completely enters the soil trench, and the resistance tends to be stable.
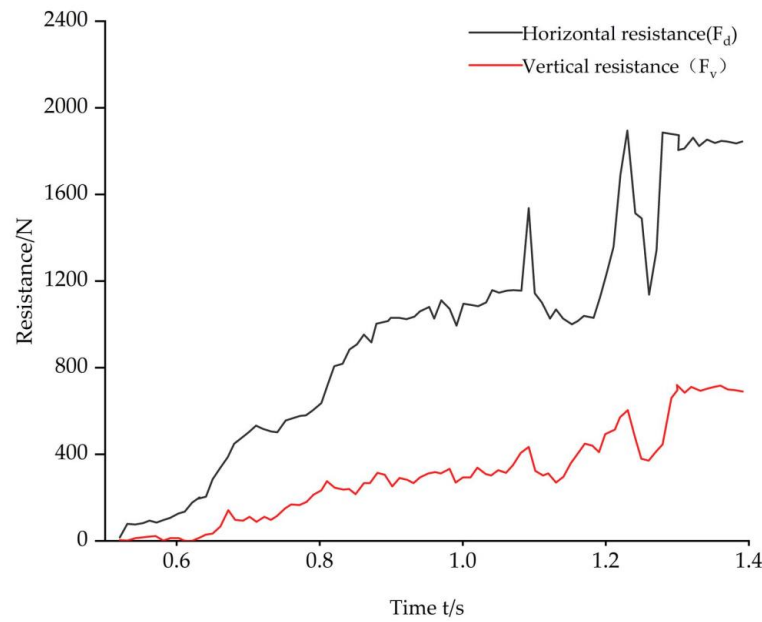
Figure 9. Resistance curve of the virtual operation in the simulation process.

3.2. Effects of Soil-Loosening Shovel Wing Opening Angle (α) and Inclination Angle (β) on Resistance

The influence of the soil-loosening shovel wing opening angle (α) on resistance is illustrated in Figure 10a. With the increase in the α, the disturbance range of the soil-loosening shovel wing increases, the number of broken soil bonds increases, the horizontal resistance (F_d) also increases, and the vertical component of the soil on the soil-loosening shovel wing rises. When the opening angle increases to 110°, the vertical resistance reaches its peak. With the increase in opening angle, the vertical resistance (F_v) shows an increment, but the increase is small.
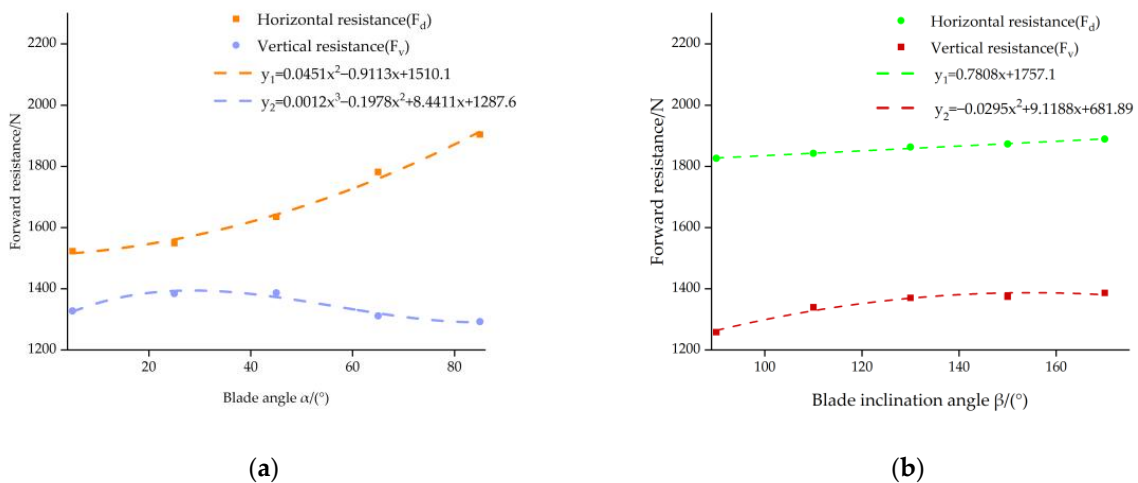

(**a**)   (**b**)

Figure 10. The law of influence of the opening angle (*β*) and inclination angle (*β*) on resistance: (**a**) effect of the soil-loosening shovel opening angle, *α*, on resistance; (**b**) influence of the soil-loosening shovel inclination angle, *β*, on resistance.

Figure 10b presents the influence of the wing inclination angle, *β*, on the resistance of the soil-loosening shovel. With the increase in *β*, the vertical cross-sectional area of the soil-loosening shovel wing increases, and the soil disturbance is enhanced, which destroys the soil bonds in a large area [49]. As a result, the horizontal resistance (F_d) of the soil-loosening shovel wing increases sharply, and the horizontal cross-sectional area of the

soil-loosening shovel wing increases, increasing the vertical component of the soil on the soil-loosening shovel. When the inclination angle exceeds 45°, the horizontal cross-sectional area of the soil-loosening shovel wing decreases, the vertical component of the soil on the soil-loosening shovel wing decreases, and the vertical resistance (F_v) reaches its peak at 45°. When the inclination angle is over 65°, the vertical resistance tends to be stable, and the change can be ignored.

In order to explore the optimal parameters of the soil-loosening shovel wing structure, the mechanical model between the soil-loosening shovel wing and soil was established to carry out the force analysis of the soil-loosening shovel wing. The spatial rectangular coordinate system *Oxyz* was established at any point on the surface of the soil-loosening shovel wing. The *y*-axis is the forward direction of the soil-loosening shovel wing during operation, the *z*-axis is the vertical direction, and the *x*-axis is vertical to the *y*-axis in the horizontal plane. The forces of the soil-loosening shovel wing in contact with the soil particles were analyzed, including the soil support force acting on the soil-loosening shovel wing (*N*; the angle to the *z*-axis is $90° - \alpha/2$), the soil friction force (*f*) acting on the soil-loosening shovel wing (on the *yz* plane), and its own gravity (*G*). The resultant force on the soil-loosening shovel wing is the resistance F_y of the soil-loosening shovel wing, whose direction is opposite to its forward direction, as shown in the Figure 11. The equilibrium equation can be obtained as follows:
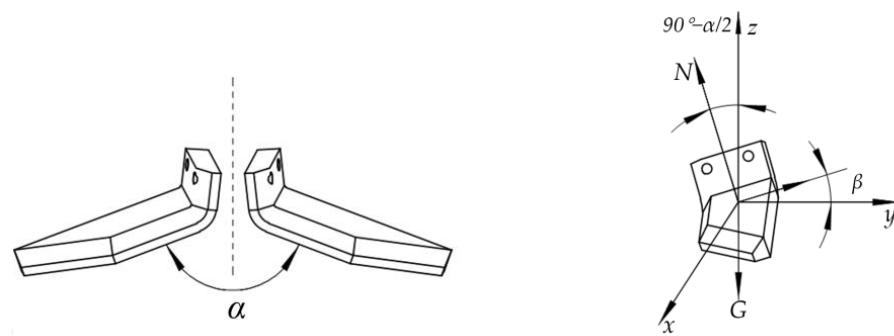

Figure 11. Mechanical analysis of the soil-loosening shovel wing.

According to the mechanical analysis, the following can be obtained:

$$N \sin\left(\frac{\alpha}{2}\right) \cos\beta + f \sin\beta = G \tag{11}$$

$$f = \mu_2 N \tag{12}$$

$$F_y = f \cos\beta - N \sin\left(\frac{\alpha}{2}\right) \sin\beta \tag{13}$$

Substituting Equations (11) and (12) into Equation (13), we obtain the following:

$$F_y = \left(\mu_2 \cos\beta - \sin\left(\frac{\alpha}{2}\right) \sin\beta\right) \frac{G}{\sin\left(\frac{\alpha}{2}\right) \cos\beta + \mu \sin\beta} \tag{14}$$

where *N* is the soil supporting force acting on the soil-loosening shovel wing, N; α is the opening angle (°); β is the inclination angle (°); *G* is the gravity of the soil-loosening shovel, N; and μ_2 is the friction coefficient between the soil-loosening shovel wing and soil.

According to Equation (14), the resistance (Fy) is related to the opening angle (α) and inclination angle (β) [50].

According to the requirements of carrot planting patterns and agronomy in Heilongjiang Province [51], as shown in the Figure 12, the length of carrot roots is 150 mm, the penetrating depth of the soil-loosening shovel is 250 mm, the width of the soil-loosening shovel wing is 180 mm, and the thickness of the soil-loosening shovel wing is 10 mm. With

the increase in the installation height of the scarifier wing, the soil disturbance coefficient presents a trend of increasing first and then decreasing; therefore, the installation height of the soil-loosening shovel wing is taken as 75 mm.
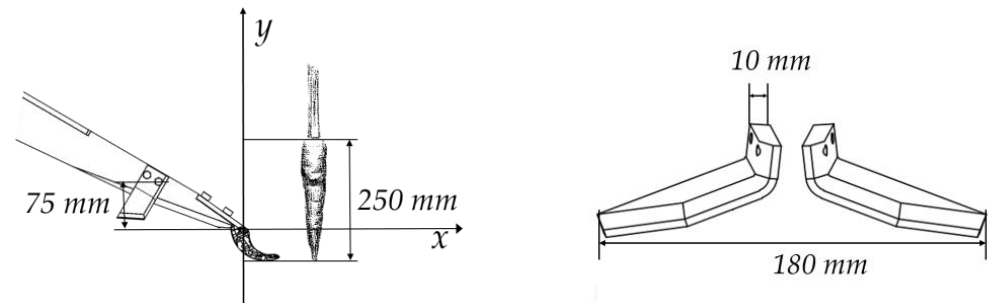

Figure 12. Geometry of the soil-loosening shovel tip.

3.3. Effects of Soil-Loosening Shovel Wing Opening Angle (α) and Inclination Angle (β) on Carrot-Pulling Force

The effects of the opening angle (α) and inclination angle (β) on the carrot-pulling force are shown in the Figure 13. With the increase in α, the soil-loosening area of the soil-loosening shovel wing increases, and the carrot-pulling force decreases. When α is greater than 150°, the soil-loosening shovel wing touches the carrot surface, causing damage. With the increase in β, the vertical cross-sectional area of the soil-loosening shovel wing increases, the soil disturbance is enhanced, and the carrot-pulling force decreases, which is conducive to reducing the missing carrot rate. When β is greater than 25°, the carrot-pulling force is less than the peak pulling force of the carrot tassel junction, meeting the requirements of carrot combine harvesting.
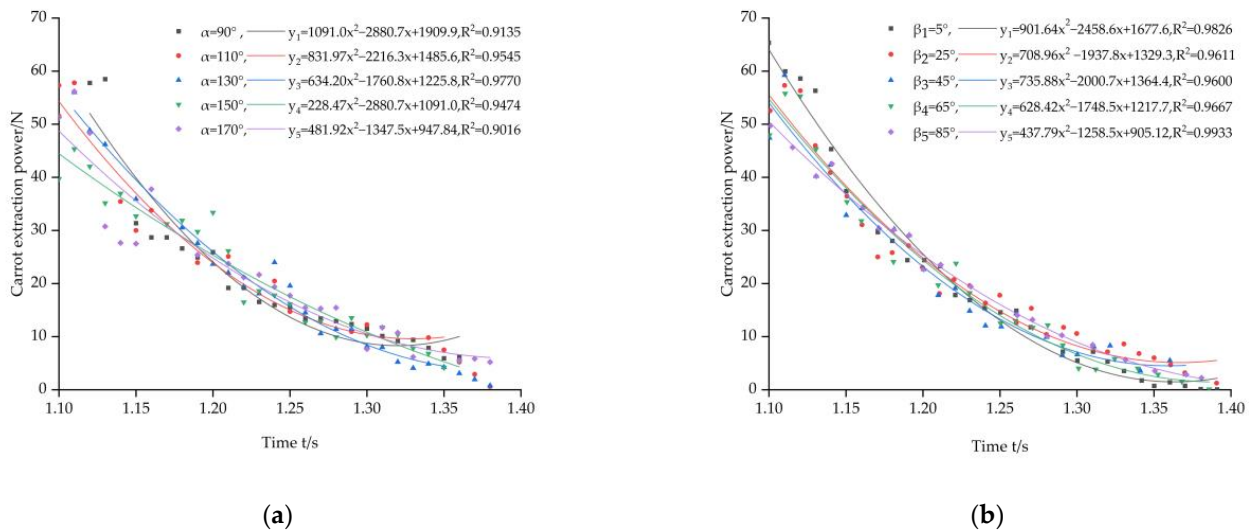

(**a**)

(**b**)

Figure 13. The influence of the opening angle and inclination angle on the carrot extraction power: (**a**) effect of the soil-loosening shovel opening angle (α) on the carrot-pulling force; (**b**) effect of the soil-loosening shovel inclination angle (β) on the carrot-pulling force.

To sum up, in order to obtain the optimal parameter combination of test factors, the opening angle, α, of (110~150°) and the inclination angle, β, of (25~65°) were selected as the value ranges of the test factors, providing a theoretical basis for the subsequent multi-factor tests.

3.4. Effects of Soil-Loosening Shovel Wing Opening Angle (α) and Inclination Angle (β) on Soil Disturbance Rate

The evaluation index of the soil disturbance rate is the change in soil bulkiness. At 0.5 s, the soil-loosening shovel starts to move, as shown in Figure 14a, and the soil plane is demarcated. At 1.1 s, part of the soil-loosening shovel wing enters the soil, and a slight uplift occurs on the soil surface, as shown in Figure 14b. At 1.3 s, the soil-loosening shovel completely penetrates the soil, as shown in Figure 14c. The EDEM section tool was used to measure the number of soil particles above the original plane of the soil, so as to obtain the amount of disturbance caused by the soil-loosening shovel under different levels, which could be converted into soil bulkiness [52]. In order to ensure the accuracy of the data, each group of soil-loosening shovels was measured three times to take an average data value.
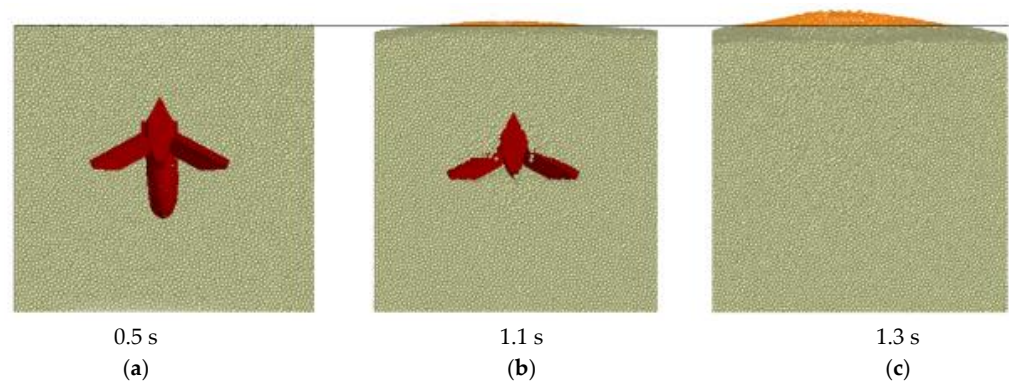

| 0.5 s | 1.1 s | 1.3 s |
| (**a**) | (**b**) | (**c**) |

Figure 14. Soil disturbance measurement: (**a**) original plane of the soil, (**b**) slight disturbance, and (**c**) change in soil bulkiness.

During the simulation, the kinetic energy of the disturbed soil particles is reflected by the color of the soil particles [53]. With the increase in the opening angle (α), the vertical cross-sectional area of the soil-loosening shovel fluctuates, the soil disturbance properties fluctuate stably, and the kinetic energy of the soil particles fluctuates. As shown in Figure 15, with the increase in the inclination angle (β), the vertical cross-sectional area of the soil-loosening shovel wing increases, the soil disturbance is enhanced, and the kinetic energy of the soil particles increases.
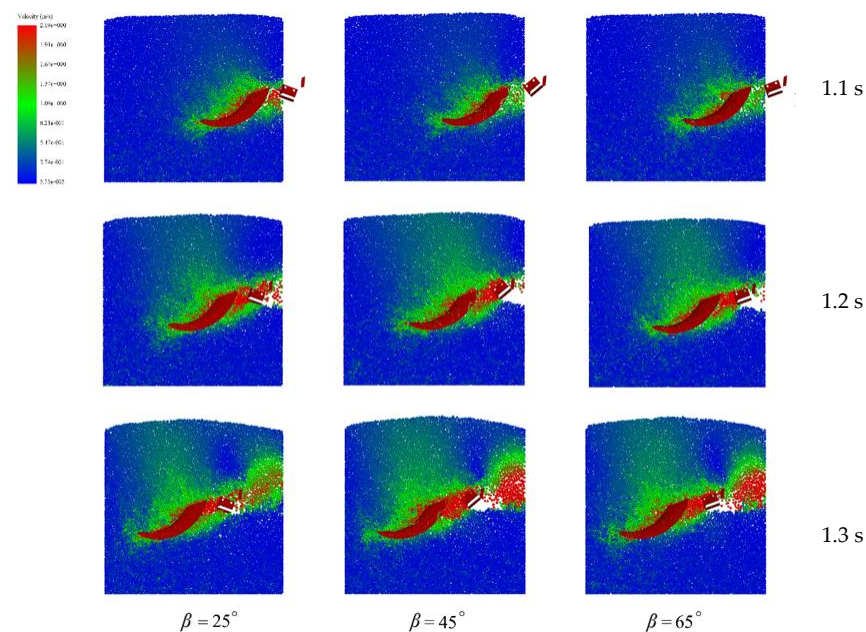

Figure 15. Changes in the soil particle kinetic energy under different inclination angles, β.

3.5. Optimum Parameters of Opening Angle (α) and Inclination Angle (β)

In order to explore the performance of the scarifier under the interaction of the opening angle (α) and inclination angle (β) and obtain the optimal structural parameter combination of the soil-loosening shovel, Design-Expert 8.0.6 software was used to design the two-factor and five-level quadratic orthogonal rotation combination test scheme. The EDEM postprocessing module was used to continuously record the resistance of the soil-loosening shovel and carrot-pulling force of the carrot combine harvester when operating under stable working conditions in a virtual soil trench.

Other parameters remained unchanged, and the average value of the data was taken as the test result. The specific test scheme and results are listed in the Table 5, where x_1 and x_2 are the factor coding values. Using Design-Expert 8.0.6 software, regression analysis and factor variance analysis were performed on the test data to select the significant influencing factors. The regression equations between the resistance (F_3) and carrot-pulling force (F_4) and factor coding values are expressed as follows:

$$F_3 = 1921.12 + 205.49x_1 + 139.23x_2 + 120.61x_1x_2 + 110.62x_1^2 + 102.15x_2^2 \quad (15)$$

$$F_4 = 49.89 - 7.73x_1 - 7.25x_2 + 8.42x_1x_2 + 3.19x_1^2 - 0.40x_2^2 \quad (16)$$

Table 5. Schemes and results of experiments.

Number	Test Factor		Performance Index	
	Opening Angle, x_1	Inclination Angle, x_2	Resistance/N	Carrot-Pulling Force/N
1	−1	−1	2236.73	91.34
2	1	−1	2366.28	75.34
3	−1	1	2209.77	67.68
4	1	1	2821.75	75.36
5	−1.414	0	1962.57	65.33
6	1.414	0	2550.63	68.68
7	0	−1.414	1972.35	61.37
8	0	1.414	2456.97	58.28
9	0	0	1920.66	49.32
10	0	0	1921.72	49.12
11	0	0	1923.36	49.76
12	0	0	1919.81	49.68
13	0	0	1923.69	49.15
14	0	0	1928.74	49.71
15	0	0	1923.55	49.81
16	0	0	1922.39	49.73

Design-Expert 8.0.6 software was used to obtain the index–factor response surface, as shown in Figure 16. As can be seen in Figure 16a, when the opening angle (α) is constant, the resistance increases with the increase in the inclination angle (β). When the inclination angle, β, is constant, the resistance increases with the increase in the opening angle, α. The resistance presents more significant changes when the inclination angle, β, changes; thus, the inclination angle (β) is the main factor affecting the resistance. As can be concluded from Figure 16b, when the opening angle, α, is constant, the moving cross-sectional area of the soil-loosening shovel wing increases with the increase in inclination angle, β, with enhanced disturbance and decreased carrot-pulling force. When the inclination angle (β) is constant, the horizontal area of the soil-loosening shovel wing increases with the increase in the opening angle (α), and the carrot-pulling force decreases. When the inclination angle (β) changes, the carrot-pulling force varies more significantly; thus, the inclination angle (β) is the main factor affecting the carrot-pulling force.
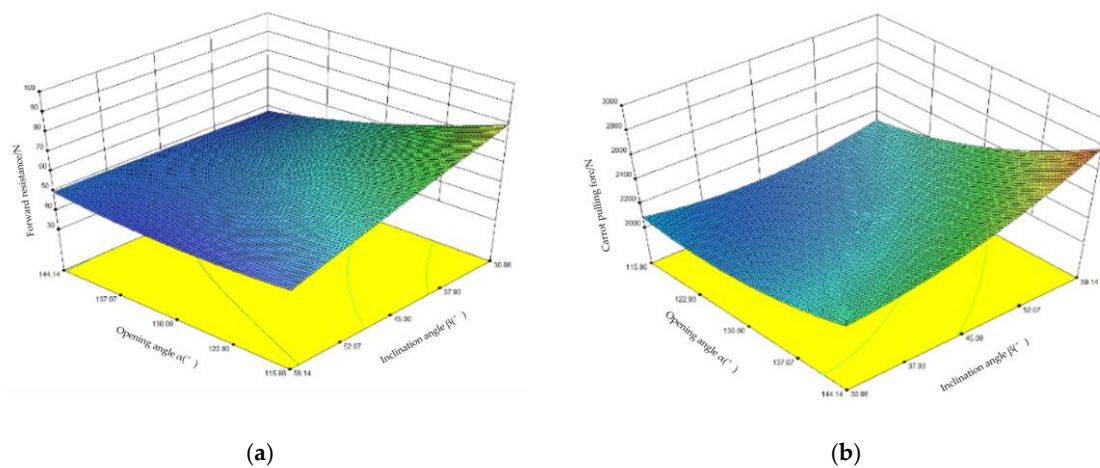
(**a**)   (**b**)

Figure 16. Influence of the experiment factors on the indexes: (**a**) the influence of the opening angle (α) and inclination angle (β) on the response surface of the resistance; (**b**) the influence of the opening angle (α) and inclination angle (β) on the response surface of the carrot-pulling force.

Combined with the boundary conditions of the test factors, and following the principle of drag reduction and disturbance increase (reducing resistance and carrot-pulling force), the resistance and carrot-pulling force regression equations of the machine were analyzed, and a nonlinear programming parameter model was established:

$$
\begin{cases}
\min F_3 \\
\min F_4 \\
s.t. \begin{cases}
0 \leq \alpha \leq 180° \\
0 \leq \beta \leq 90° \\
0 \leq F_3 \leq 3000N \\
0 \leq F_4 \leq 56N
\end{cases}
\end{cases}
\tag{17}
$$

Design-Expert 8.0.6 software was used to analyze and solve the established mathematical model. A set of reasonable parameter combinations was selected from the optimization results; that is, when the opening angle (α) is 127.27° and inclination angle (β) is 47.37°, the comprehensive operation performance of the machine is better, with a resistance of 1923.35 N and a carrot-pulling force of 49.53 N. According to the optimization results, the virtual simulation verifies that the resistance is 1908.76 N and the carrot-pulling force is 48.37 N, which is basically consistent with the optimization results.

3.6. Missing Carrot Rate under Optimal Parameters

To carry out the carrot-harvesting experiment, α was set to 125°, β was set to 45°, and the speed was set to 2.88 km/h. Five ridges of carrots were selected for harvesting, where each ridge was 100 m long, and the number of missing carrots on each ridge was counted. The harvest data of carrot are shown in Table 6.

Table 6. Missing-carrot rate.

Serial Number	Number of Missing Carrots	Total Number of Carrots	Missing-Carrot Rate (%)
1	19	526	3.6
2	41	542	7.5
3	24	493	4.8
4	38	587	6.4
5	27	506	5.3
Average			5.52

It can be seen from the table that, under the optimal parameter conditions, the missed pulling rate of carrots is only 5.52%, which meets the operating requirements of carrot combine harvesters.

4. Conclusions

In this study, we developed an efficient drag-reducing bionic soil-loosening shovel based on the bionic design of the badger claw toe structure and carried out virtual simulation tests. The experimental results show that the operating speed, opening angle, and inclination angle of the shovel wing are the main factors affecting the performance of the bionic shovel.

(1) The national standard test method was used to determine the physical parameters of the soil texture, firmness, and water content of the test field. At the same time, carrot geometric parameters and related mechanical parameters were determined.

(2) The drag-reducing bionic soil-loosening shovel was designed with the badger claw toe as the bionic prototype, and its drag-reducing mechanism was analyzed. The mechanical contact model between the soil-loosening shovel wing and soil was established to explore the mechanical law between the soil-loosening shovel wing and soil. The structural parameters of the soil-loosening shovel wing affecting the working performance were determined, which were the opening angle (α) and the inclination angle (β). Through the mechanical analysis, it was found that the resistance of the soil-loosening shovel increases with the increase in working speed.

(3) The discrete element method was applied to establish the component–carrot–soil particle multivariate simulation model, with the opening angle (α) and inclination angle (β) as the test factors; and the resistance, carrot-pulling force, and soil particle disturbance rate served as the test indexes. The mathematical model between the factors and indexes was established using the virtual orthogonal test method. The optimization model was built using the multi-objective variable optimization method. It is concluded that the optimal parameter combination of the soil-loosening shovel is an opening angle (α) of 120.27° and an inclination angle (β) of 47.37°.

In a word, the high-efficiency drag-reducing bionic soil-loosening shovel has a better working performance and better drag reduction characteristics than traditional soil-loosening shovels, which can effectively solve the problems of the low soil disturbance, high resistance, and high missing carrot rate of the soil-loosening shovels used on carrot combine harvesters. At the same time, it can improve the quality and efficiency of carrot combine harvesting and meet the agronomic requirements of carrot harvesting.

Nomenclature

S_m	Soil water content
m_0	Mass of empty soil box
m_1	Total mass of soil and box before drying
m_2	Total mass of soil and box after drying
d_{vi}	Soil bulk density of the ith soil sample
V	Cutting ring volume
M_i	Mass of the ith soil sample
W_i	Soil water content
σ_i	Tensile strength of the ith carrot root
F_i	Peak pulling force of the ith carrot tassel junction fracture
D_i	Diameter of the ith carrot tassel junction fracture
y	Soil disturbance coefficient
A_s	The cross-sectional area from the ground surface to the real bottom of trench after subsoiling
A_q	The cross-sectional area from the ground surface to the theoretical bottom of trench before subsoiling
m	Particle mass
v	Initial operating speed
v_0	Final forward velocity
t	Action time
a	Acceleration
μ_1	Friction coefficient between bionic soil-loosening shovel and soil
N	Soil supporting force acting on soil-loosening shovel wing
α	Opening angle
β	Inclination angle
G	Gravity of soil-loosening shovel
μ_2	Friction coefficient between soil-loosening shovel wing and soil

References

1. Li, K.; Yang, B.; Yang, W.; Shang, S.; Li, J.; Yang, D.; Jia, J. Planting Status and Research Progress on Seeding Machine of Carrot at home and Abroad. *Agric. Eng.* **2015**, *5*, 1–5.
2. Yang, W.; LI, J.; Gao, B.; Shang, S.; Li, K.; Cui, H. Current situation and thinking of carrot planting and harvesting mechanization. *Agric. Mech. Res.* **2014**, *36*, 247–252.
3. Jin, W.; Xiang, L.; Peng, G.; Ming, N.; Qi, W.; Wen, Z. Design and Experiment of High Efficiency Drag Reducing Shovel for Carrot Combine Harvester. *Trans. Chin. Soc. Agric. Mach.* **2020**, *51*, 93–103.
4. Chong, Z.; Xu, F.; Hu, W.; Xueg, Z.; Xue, Y. Structural Design and Drag Reduction Test of Wedge Self-lubricating Deep Easing Shovel. *J. Agric. Mech. Res.* **2021**, *43*, 78–83.
5. Askari, M.; Shahgholi, G.; Abbaspour-Gilandeh, Y.; Shamsabadi, H. The effect of new wings on subsoiler performance. *Appl. Eng. Agric.* **2013**, *32*, 353–362.
6. Cheng, H.; Yu, H.; Wei, L. Influencing factors and reduction strategies of subsoiling tillage resistance. *J. Northwest AF Univ.* **2016**, *44*, 202–208.
7. Aday, H.; Hilal, Y. The effect of lifting angle of the subsoiler foot wings on its field performance in heavy soils. *Iraqi J. Agric.* **2004**, *9*, 195–207.
8. Wei, H.; Liu, D.; Fu, M.; Zhou, D.; Wu, B. Design and DEM Analysis of Bionic Drag-reducing Slant Column Subsoilers. *Agric. Eng.* **2022**, *12*, 84–88.
9. Qiu, Z.; Zhang, H.; Zhang, F.; Mao, P.; Ma, Y. Simulation analysis of Corrugated bionic deep slooping Shovel based on Finite element Method. *Jiangsu Agric. Sci.* **2018**, *46*, 201–203.
10. Gowripathi, N.N.V.R.; Chaudhary, H.; Sharma, A.K. Kinematic analysis of bionic vibratory tillage subsoiler. In *Advances in Engineering Design*; Springer: Singapore, 2018; pp. 187–195.
11. Li, B.; Chen, Y.; Chen, J.J.S.; Research, T. Modeling of soil–claw interaction using the discrete element method (DEM). *Soil Tillage Res.* **2016**, *158*, 177–185. [CrossRef]
12. Zhang, Z.; Gan, S.; Zuo, G.; Tong, J. Bionic Design and Performance Experiment of Sandfish Head Inspired Subsoiler Tine. *Nongye Jixie Xuebao/Trans. Chin. Soc. Agric. Mach.* **2021**, *52*, 33–42.
13. Q, E.B. Evaluación numérica de un subsolador biónico inspirado en el armadillo de nueve bandas (Dasypus novemcinctus). *Inst. De Ing. Y Tecnol.* **2019**.
14. Zhang, J.; Tong, J.; Ma, Y. Design and Experiment of Biomimetic Drag Reduction Deep Loose Shovel. *Trans. Chin. Soc. Agric. Mach.* **2014**, *45*, 141–145.

15. Osuna-Ceja, E.S.; Garibaldi Márquez, F.; García Hernández, R.V. Performance of a biomimetic integral subsoiler for sustainable tillage of agricultural soils. *Acta Univ.* **2019**, *29*, e1968.
16. Zhang, P.; Guo, Z.; Jin, X.; Guo, Z.; Zhang, S. Design and experiment of bionic subsoiler with variable variable curvature share shaft drag reduction. *J. Jilin Univ.* **2022**, *52*, 1174–1183.
17. Wang, X.; Yue, B.; Gao, X. Discrete Element Simulations and Experiments of Disturbance Behavior as Affected by Mounting Height of Subsoiler's Wing. *Trans. Chin. Soc. Agric. Mach.* **2018**, *49*, 124–136.
18. Kornel, T.; Istvan, J.J.; Mouazen, A.M. Modelling soil-sweep interaction with discrete element method. *Soil Tillage Res.* **2013**, *134*, 243–258.
19. Ucgul, M.; Fielke, J.M.; Saunders, C. 3D DEM tillage simulation: Validation of a hysteretic spring (plastic) contact model for a sweep tool operating in a cohesionless soil. *Soil Tillage Res.* **2014**, *144*, 220–227. [CrossRef]
20. Hu, Y.; Li, M.; Ren, H.; Si, B. Measurement of soil water content using distributed temperature sensor with heated fiber optics. *Trans. Chin. Soc. Agric. Eng.* **2019**, *35*, 42–49.
21. Gao, J.; Ma, Y.; Luo, F. Soil moisture monitoring Technology Based on resistivity imaging. *J. Arid Land Resour. Environ.* **2019**, *33*, 190–196.
22. Qu, F.; Li, W. Optimal Design and Research on Soil Stratified Sampling Device Based on ANSYS. *Mech. Eng.* **2015**, *8*, 10–12.
23. Cui, Y.; Shi, Y.; Zhu, M. Measurement of grain and soil bulk density. *China Metrol.* **2014**, 99–100.
24. Gao, G. Discussion on improvement of soil bulk density measurement method of forest land. *Biotechnol. World* **2012**, *10*, 16–17.
25. Hang, C.; Zhang, P.; Li, W. Experimental research on influence of rake angle on soil hardness variation under sub-soilin. *Chin. J. Agric. Mech.* **2016**, *37*, 36–40.
26. Han, F.; Chen, H.; Ren, K. Dun Guoqiang. Study on physical and mechanical properties of the carrot in north. *J. Northeast Agric. Univ.* **2012**, *43*, 36–41.
27. Chen, H.; Ren, K.; Yu, J. Experimental study on Physical and Mechanical Properties of Carrot. *Chin. Soc. Agric. Eng. Chin. Soc. Agric. Eng.* **2009**, 1360–1364.
28. Liu, Z.; Wang, J.; Dai, Q.; Zhang, J.; Zhao, G. Experimental study on geometric parameters and mechanical properties of carrot based on digging and plucking. *J. Agric. Mech. Res.* **2021**, *43*, 176–179+185.
29. Zeng, G. *Research on Mechanical Properties of Carrot Tassels and Pull Harvesting Parts*; Zhejiang Sci-Tech University: Hangzhou, China, 2017.
30. Liu, Q.; Tian, C.; Xu, L. Effect of Soil Physical Properties on Mechanical Pulling Process of Carrot. *Agric. Eng.* **2019**, *9*, 63–66.
31. Wang, L.; Li, Y.; Zhang, M. Report on Reproductive Behavior and Cycle of Captive Badger. *Chin. J. Zool.* **2015**, *50*, 957–962.
32. Gu, Y. Special economic animal breeding of badgers China Livest. *Poult. Breed.* **2015**, *11*, 76.
33. Ma, Z.; Tan, W.; Huo, Q. Design of bionic Deep Loose Shovel Tip based on 3D printing. *Hebei Agric. Mach.* **2020**, *1*, 16–17.
34. Wang, W. Application Research of Reverse Engineering in the Product Bionics Design. *Packag. Eng.* **2011**, *32*, 36–39.
35. Li, S.; Tong, J.; Zhang, S.; Chen, B.C. Reverse Engineering and Engineering Bionics. *Trans. Chin. Soc. Agric. Mach.* **2004**, 109–112.
36. Yu, J.; Wang, R.; Tong, X. Reconstruction of Rabbit's claw toe Surface and Extraction of Feature Curve. *Chin. J. Agric. Mech.* **2019**, *40*, 43–47.
37. Fu, W.; Chen, H.; Kan, Z. Optimizing parameters on vibration breakshovel of radish harvester. *Trans. CSAE* **2011**, *27*, 46–50.
38. Barr, J.B.; Ucgul, M.; Desbiolles, J. Simulating the effect of rake angle on narrow opener performance with the discrete element method. *Biosyst. Eng.* **2018**, *171*, 1–15. [CrossRef]
39. Liu, K.; Su, H.; Li, F. Parameter calibration of soil discrete element model based on response surface method. *Chin. J. Agric. Mech.* **2021**, *42*, 143–149.
40. Wang, X.; He, H.; Chen, W. Soil model parameter calibration method based on discrete element. *Trans. Chin. Soc. Agric. Mach.* **2017**, *48*, 78–85.
41. David, A.H. *Application of DEM to Micro-Mechanical Theory for Large Deformations of Granular Media*; University of Michigan: Ann Arbor, MI, USA, 1997.
42. Li, C. *Study on the Extraction Force of Carrot Based on EDEM*; Shandong Agricultural University: Taian, China, 2018.
43. Li, X.; Zhang, D.; Wang, W.; Cui, T. Performance parameter optimization and experiment of forced-vibration subsoiler. *Trans. Chin. Soc. Agric. Eng.* **2015**, *31*, 17–24.
44. Li, W. *Study on the Effect of Stratified Subsoiling on Soil Disturbance*; Northwest A & F University: Xianyang, China, 2017.
45. Huang, Y.; Hang, C.; Yuan, M.; Wang, B. Discrete element simulation and experiment on disturbance behavior of deep loose soil. *Trans. Chin. Soc. Agric. Mach.* **2016**, *47*, 80–88.
46. Han, X.; Chen, H.; Dun, G. Current Situation Analysis of Carrot Harvesting Mechanization. *Agric. Mech. Res.* **2015**, *37*, 259–263.
47. Li, K. *Research on Key Technologies of Self-Propelled Carrot Combine Harvester*; Chinese Academy of Agricultural Mechanization Sciences: Chaowai, China, 2015.
48. Wang, J.; Shang, S. Development and test of self-propelled double-row carrot combine harvester. *J. Agric. Eng.* **2012**, *28*, 38–43.
49. Liu, J. *Research on Parameter Optimization of Subsoiling Shovel and Comprehensive Effect of Loosening Soil Based on Discrete Element Method*; China Agricultural University: Guangzhou, China, 2018.
50. Xia, L. *Parameter Optimization and Experimental Research on Subsoiling Shovel Wing Based on Discrete Element Method*; Northwest A & F University: Xianyang, China, 2018.
51. Chen, D. Carrot planting technology. *Mod. Anim. Husb. Sci. Technol.* **2020**, 31–32.

52. Yue, B. *Discrete Element Simulations and Experiments on the Influence of Stratified Subsoiling on Soil Disturbance*; Northwest A & F University: Xianyang, China, 2019.
53. Chen, G.; Xu, C.; Guo, Y. Establishment of Particle Dynamics Model. *Comput. Appl. Chem.* **2000**, *6*, 505–508.